Contents list available at CBIORE journal website

International Journal of Renewable Energy Development

Journal homepage: https://ijred.cbiore.id

Research Article

Effects of CaO addition into $CuO/ZnO/Al_2O_3$ catalyst on hydrogen production through water gas shift reaction

Zulaicha Dwi Hastuti, Erlan Rosyadi*, Hana Nabila Anindita, Imron Masfuri, Nurdiah Rahmawati, Tyas Puspita Rini, Trisno Anggoro, Wargiantoro Prabowo, Frendy Rian Saputro, Ade Syafrinaldy

Research Center for Energy Conversion and Conservation, National Research and Innovation Agency (BRIN), South Tangerang, Indonesia

Abstract. Hydrogen is a promising renewable energy carrier and eco-friendly alternative to fossil fuels. Water-gas-shift reaction (WGSR) is commonly used to generate hydrogen from renewable biomass feedstocks. Enriching hydrogen content in synthesis gas (syngas) production can be made possible by applying the WGSR after gasification. WGSR can achieve a maximal carbon monoxide (CO) conversion using a commercially patented CZA ($Cu/ZnO/Al_2O_3$) catalyst. This study proposed three in-lab self-synthesized CZA catalysts to be evaluated and compared with the patented catalyst performance-wise. The three catalysts were prepared with co-precipitation of different Cu:Zn:Al molar ratios: CZA-431 (4:3:1), CZA-531 (5:3:1) and CZA-631 (6:3:1). The catalysts characteristics were determined through X-ray diffraction (XRD), Brunauer-Emmett-Teller (BET) analysis and Scanning Electron Microscopy (SEM) techniques. CO gas was mixed with steam in a catalytic reactor with a 3:1 molar ratio, running continuously through the catalyst at 250 °C for 30 mins. All three catalysts, however, performed below expectations, where CZA-431 had a CO conversion of 77.44%, CZA-531 48.75%, and CZA-631 71.67%. CaO, as a co-catalyst, improved the performance by stabilizing the gas composition faster. The CO conversion of each catalyst also improved: CZA-431 improved its CO conversion to 97.39%, CZA-531 to 96.71%, and CZA-631 to 95.41%. The downward trend of the CO conversion was deemed to be caused by copper content found in CZA-531 and CZA-631 but not in CZA-431, which tended to form a Cu-Zn metal complex, weakening the catalyst's activity.

Keywords: syngas, hydrogen, water-gas-shift reaction, CO conversion, catalyst, $Cu-Zn-Al_2O_3$, CaO

Received: 28th Oct 2023; Revised: 26th April 2024; Accepted: 15th May 2024; Available online: 23rd May 2024

1. Introduction

The Indonesia government is promoting using biomass for energy to support clean energy transition program, particularly achieving Indonesia's renewable energy targets of 23% by 2025 (RI 2014). In the quest for achieving such targets and seeking sustainable energy solutions to address the issues of greenhouse gas emissions and energy security, hydrogen has emerged as a suitable secondary energy source and promising clean energy carrier due to its high energy efficiency, high calorific value, and environmentally friendly nature, with the potential to revolutionize a wide range of sectors, including transportation, industry, and power generation (Aziz, Darmawan, & Juangsa 2021; Veziroğlu & Şahi˙n 2008). Emissions emitted by hydrogen are lower compared to other commercial or drop-in fuels (Speight 2019; Watanabe *et al.* 2022). H_2 can be utilized for various purposes, from energy storage utilities to prospective transport fuel (Nagar *et al.* 2023; Saeidi *et al.* 2017). It has also been commonly used in refineries as essential feedstock (Al-Baghdadi, Ahmed, & Ghyadh 2023; Damayanti, Sarto, & Sediawan 2020; Ratnawati *et al.* 2022).

Unfortunately, the availability of H_2 is not particularly natural for energy use. Most of the H_2 in the world can only be created or produced synthetically (Shuai *et al.* 2015; Stiegel & Ramezan 2006). Nowadays, steam reforming is capitalizing 95% of the captive market of synthetic H_2 production, despite the non-sustainable characteristic of the process (Pal *et al.* 2018; Sahrin *et al.* 2022), followed by water splitting via electrolysis (4%) (Arregi *et al.* 2018; Pal *et al.* 2018). Nevertheless, steam reforming utilizes fossil and carbonaceous materials up to 96% as feedstock, predominantly natural gas (48%) and oil (30%), which renders the process unsustainable (Arregi *et al.* 2018). Despite the clean characteristics of hydrogen, the unsustainable characteristics of its production process will impair the initial idea of hydrogen application to reduce carbon emissions. As the world transitions towards a low-carbon future and the need to develop clean and sustainable energy sources increases significantly, hydrogen production from renewable sources has gained increasing attention worldwide due to its ability to decarbonize energy systems, reduce greenhouse gas emissions, and minimize dependence on fossil fuels (Yana *et al.* 2022). Consequently, this condition urges the utilization of renewable and more environmentally friendly feedstock in hydrogen production.

Among the various pathways for hydrogen production, biomass stands out as a promising, abundant, versatile, and widely available resource. Biomass is promising as a renewable energy source that may be easily obtained in Indonesia from

* Corresponding author
Email: erla003@brin.go.id (E.Rosyadi)

https://doi.org/10.61435/ijred.2024.59257
ISSN: 2252-4940/© 2024.The Author(s). Published by CBIORE

agricultural, plantation, forest areas, and industrial waste such as palm oil, sugarcane, tapioca, pulp and paper, wood, and rice (Pambudi *et al.* 2023; Yana *et al.* 2022). Biomass is considered a neutral carbon source since photosynthesis captures carbon from CO_2 in the air (He *et al.* 2023). It also can be renewed in the short term, giving it considerable potential to be utilized as feedstock in hydrogen production, which can later be notated as biohydrogen. The International Energy Agency (IEA) also underlines the considerable potential of biohydrogen in decreasing greenhouse gas emissions and encouraging growth in hydrogen production from renewable sources.

Biohydrogen production based on biomass feedstock is mainly conducted via thermochemical and biological routes (Kalinci, Hepbasli, & Dincer 2009), which later is considered a time-consuming and inefficient process (Chen *et al.* 2023; Ghodke *et al.* 2023; Peng *et al.* 2017). The main thermochemical methods for the conversion of biomass into hydrogen-rich gas are gasification, pyrolysis, and aqueous phase reforming (Duman & Yanik 2017; Heidenreich & Foscolo 2015; Huber, Iborra, & Corma 2006; Lepage *et al.* 2021; Muharto *et al.* 2023; Tian *et al.* 2024). Biohydrogen-based microalgae, involving biophotolysis, is also starting to develop (Sahrin *et al.* 2022; Wang *et al.* 2021). The cheapest method for producing H_2 (2 US$/kg) is the thermochemical method of gasification, followed by dark fermentation in the biological method (2.3 US$/kg) (Ghodke *et al.* 2023). Compared to chemical and biochemical methods, the thermochemical method offers a more straightforward approach, high efficiency, and low-cost production to hydrogen generation (Lanjekar, Panwar, & Agrawal 2023). It typically does not necessitate the addition of chemical agents, and it can also convert a diverse range of wet biomass and use the feedstock obtained from biomass (Dou *et al.* 2019). Thus, the thermochemical process has been considered the most promising technology for hydrogen production from biomass (Agaton, Batac, & Reyes Jr 2022; Dou *et al.* 2019; Tleubergenova, Han, & Meng 2024; Younas *et al.* 2022).

The biomass gasification process, however, is still grappling with its technical challenges. Syngas products generally have a low hydrogen-to-carbon monoxide ratio ($H_2/CO < 1$), indicating low H_2 concentration due to changing chemical reactions based on operating conditions. Higher CO in the gas product will be the consequence of the biomass's abundance of carbonyl groups, which are simpler to bond-scission. (He *et al.* 2023). This situation seriously limits the large-scale applications of biomass-to-hydrogen technology. Employing steam instead of air as a gasifying agent can bolster the syngas production, enriched with H_2 (Acharya, Dutta, & Basu 2010), enhancing the syngas calorific value. Steam will accelerate reforming reactions and generate gasification products with the highest H_2/CO ratio and the fewest impurities like CH_4, H_2S, and NH_3 (Havilah *et al.* 2022; Sansaniwal *et al.* 2017). Without steam, the gasification product will be dominated by CH_4 and CO_2 (Watson *et al.* 2018). Steam gasification provides hydrogen's most significant stoichiometric yield, nearly three times that of air gasification. The generation of H_2 and CO_2 is greatly enhanced when the steam-to-biomass ratio (S/B) rises from 0 to 10. The yields of CO and CH_4 are almost constant at the same period. At S/B 7.5, the H_2/CO ratio reaches its maximum of 0.96, which is three times higher than the ratio in anhydrous conditions of 0.34. As S/B increases further to 10 levels, the H_2/CO ratio decreases. The increased steam levels enhanced the decomposition of tar, while simultaneously reducing the concentration of hydrocarbons in the syngas, particularly C_3-C_4 and unsaturated C_2 (Martínez *et al.* 2022; Martínez *et al.* 2020). Steam also promotes water gas shift reaction (WGSR) to occur more intensively in the biomass gasification process, shifting water vapour (H_2O) to H_2 and carbon dioxide (CO_2), harnessing the existence of CO (Younas *et al.* 2022).

Even though steam gasification gives better performance in producing a higher H_2/CO ratio in gas products, further hydrogen concentration is needed. Adding steam to syngas in a downstream catalytic reactor after gasification can also be a method to convert CO gas to H_2 and CO_2, hence increasing the H_2/CO ratio (Ostadi, Rytter, & Hillestad 2019). Comparatively, the gasification process combined with a following WGSR reaction, as shown in Figure 1, is more adaptable for large-scale applications due to its capability to continually convert feedstocks into high-value hydrogen without limiting the composition of biomass (He *et al.* 2023).

Extensive research has been conducted on WGSR to increase biohydrogen from renewable energy sources like solid waste and biomass via gasification (Ahn *et al.* 2020; Shen *et al.* 2023; Zhou *et al.* 2023). WGSR has been an essential intermediate reaction in industrial applications, especially in H_2/CO ratio adjustment of the gaseous product from methane steam reforming by removing CO and producing hydrogen (Shen *et al.* 2023). Simultaneously completing the removal of CO and H_2 production is a significant benefit of the WGSR process (Zhou *et al.* 2023). The exothermic equilibrium in WGSR depends highly on factors like operating temperature, feed composition, and the presence of a catalyst, as described by Equation (1) (Poggio-Fraccari *et al.* 2022). Thermodynamically, WGSR is more efficient at lower temperatures, but kinetically, it tends to prefer higher temperatures with different catalyst types (Dasireddy *et al.* 2020; Shen *et al.* 2023).

$$CO + H_2O \leftrightarrow CO_2 + H_2 \qquad \Delta H = -41\ kJ \qquad (1)$$

Catalysts play a vital role in achieving maximum CO conversion and efficiency of the process (Dawood, Anda, & Shafiullah 2020). Significant progress has been made in improving the WGSR process, specifically on the catalyst type. Novel catalysts utilizing nanoparticles on a supporting medium have been extensively explored. Various catalyst candidates, such as iron, copper, cobalt, gold, platinum, and rare earth metals (e.g., cerium, samarium, gadolinium, and lanthanum), were investigated and tested extensively for their potential as WGSR catalysts (Gradisher, Dutcher, & Fan 2015). Current research is focussing more on the catalyst's support and solid additives. Catalysts must be mixed or supported with other substances to prevent or slow down sulfur poisoning. WGSR is sensitive to sulfur poisoning that might cause catalyst deactivation (Baraj, Ciahotný, & Hlinčík 2021).

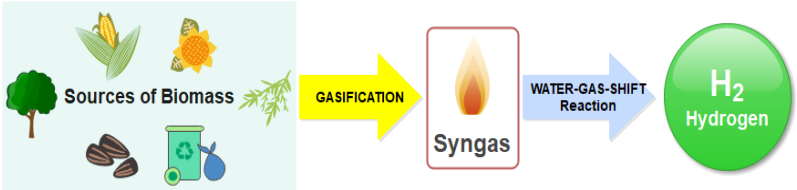

Fig. 1 Synergistic route of biomass gasification and WGSR to produce biohydrogen.

WGSR is typically classified as (1) high-temperature shift (HTS) at 300-350 °C using an iron-based catalyst which focuses on accelerating the reaction, and (2) low-temperature shift (LTS) at 200-250°C using a copper-based catalyst which focuses to remove CO gas to less than one ppm (Gogate 2020; Poggio-Fraccari *et al.* 2022; Shen *et al.* 2023). The LTS-WGSR is more challenging to perform without a suitable catalyst. The LTS-WGSR catalyst is typically a combination of CuO, ZnO, and Al_2O_3. As an active site, copper has high selectivity and activity performance, which makes it most appropriate for WGSR at low CO concentrations and temperatures (Baraj, Ciahotný, & Hlinčík 2021). ZnO can adequately absorb sulfur from poisoning the Cu crystallites, gives solid structural support for the catalyst (Fajín & Cordeiro 2021; Pal *et al.* 2018), and increases Cu dispersion. The close interactivity of Cu and ZnO will strain the copper lattice with higher catalytic activity than bulk-structured copper (Günter *et al.* 2001). Meanwhile, Al_2O_3 makes dispersion easier and minimizes pellet shrinkage (Loganathan, & Shantha 2010). Zinc aluminate, formed when zinc and aluminium ions (Al^{3+}) react, stabilizes the highly dispersed Cu/ZnO crystallites and prevents Cu agglomeration. During the reduction and reaction stages, Cu's surface enrichment and stabilization are accelerated (Baltes, Vukojević, & Schüth 2008; Chen *et al.* 1999). The high activity of the CZA catalyst is highly attributed to metallic Cu and ZnO's synergistic interaction (Na *et al.* 2019). The catalyst activity is mainly affected by the Cu/Zn/Al ratio (Lucarelli *et al.* 2018). High Cu concentrations can further intensify the occurrence of WGSR (Gunawardana, Lee, & Kim 2009).

The relatively affordable copper-based catalysts can maximize CO gas conversion even in low temperatures (Dasireddy *et al.* 2020; Fajín & Cordeiro 2021). Although metal-based catalysts have performed excellently in LTS-WGSR (Jang *et al.* 2019; Zhu *et al.* 2019; Zhu & Wachs 2016), the high price and the tendency of active components to aggregate hinder the application in the industry (Qin *et al.* 2018; Shen *et al.* 2023; Yao *et al.* 2017). Hence, a growing interest is in developing low-cost catalysts or other catalytic techniques for enabling low-temperature WGSR (Shen *et al.* 2023; Xiang *et al.* 2020).

Calcium oxide (CaO) is a known alkaline earth metal catalyst for gasification. CaO acts as a CO_2 absorbent and tar reducer via cracking/reforming (Fan *et al.*, 2015; Zhou *et al.,* 2019). CaO breaks the p-electron cloud's stability of condensed aromatic compounds in tar (Yongbin *et al.,* 2004). It promotes the gasification reaction of char and generates more condensable products and less residual char. CaO also acts as a catalyst for WGSR and steam reforming of methane (Guoxin *et al.*, 2009). Its catalyst effect on the WGS reaction was more potent than that on the methane steam reforming (Hu and Hao, 2009). CaO will facilitate the H_2O dissociation that restricts the rate of the WGSR process (Figueiredo *et al.* 1998; Yan *et al.* 2021). CaO can also capture CO_2 before creating the $CaCO_3$ product layer (Živković *et al.* 2016). By capturing the CO_2, the WGSR might be shifted to the product side, increasing the production of H_2, especially in syngas produced from the biomass gasification process.

The commercially available CZA catalyst is renowned for performing well in WGSR to maximize the CO conversion to H_2. Nonetheless, the role of CaO as support of the catalyst and a co-catalyst has scarcely been explored. Therefore, this research investigated the impact of CaO addition on catalytic WGSR, using CZA as a catalyst in three different molar ratios of Cu:Zn:Al (4:3:1; 5:3:1; and 6:3:1) through the co-precipitation process. The main parameters of interest were the total CO conversion, the average H_2 concentration in the gas product, and the time required to reach exothermic equilibrium. A commercial CZA catalyst from Sud-Chemie (CZA-SC) was used for comparison.

2. Materials and Methods

2.1 Materials

Reagents for synthesized CZA catalysts were zinc nitrate tetrahydrate ($Zn(NO_3)_2.4H_2O$), copper (II) nitrate trihydrate ($Cu(NO_3)_2.3H_2O$), aluminium nitrate nonahydrate ($Al(NO_3)_3.9H_2O$), and sodium carbonate (Na_2CO_3) anhydrous. All the chemicals above were provided by Merck KGaA Germany and designated for analysis grade under the EMSURE® label. Merck KGaA Germany also provided calcium oxide (CaO) from marble in small lumps with assay (complexometric) ≥ 97.0%. Commercial CZA catalyst MDC-03 from Sud-Chemie was utilized as the benchmark. In this work, the WGSR utilized CO derived from the syngas produced during biomass gasification to produce hydrogen. Therefore, CO was employed as the gas model for this investigation. A mixture of steam and carbon monoxide gas was supplied to the WGSR with a ratio of 3:1.

2.2 Catalyst Preparation

The CZA catalysts were synthesized via co-precipitation method with different compositions. Precise ratios of the $Cu(NO_3)_2$, $Zn(NO_3)_3$, and $Al(NO_3)_3$ solutions were mixed to create the precursor solution and then placed in the burette. 100 mL of purified water was filled in a beaker glass and put in a water bath. The precursor solution and 1 M Na_2CO_3 solution were dripped concurrently into 100 mL of distilled water while maintaining a neutral pH and a temperature of approximately 60°C. The precipitate in the form of carbonate metal salt was left to stand for 120 minutes at 70 °C. It was filtered and rinsed with water until pH six was reached, then dried at 80 °C for 18 hours. Hydroxy-carbonate precursors (hydrotalcite-like crystals) were calcined at 330 °C for 3 hours in 100 mL/min air to produce a CZA catalyst.

Three different ratios of [$(Cu(NO_3)_2$: $Zn(NO_3)_3$: $Al(NO_3)_3$] solutions were used which are 4:3:1, 5:3:1, and 6:3:1, and the catalysts produced were notated as CZA-431, CZA-531, and CZA-631, respectively. CaO was added by physically mixing the CaO with the synthesized catalyst with the ratio 2:1 notated as CaO-CZA-431, CaO-CZA-531, and CaO-CZA-631 before being used in the reactor. The amount of catalyst loaded into the reactor would be 3 grams.

2.3 Catalyst Characterization

Both commercial and synthesized CZA catalysts involved in the experiments were characterized. The crystal-oxide formation in the catalyst was examined through Energy Dispersive X-ray diffraction Rigaku-Int 2000 X-ray generator with CuKα radiation source (Rigaku Corp., Japan), while the catalyst composition was characterized using the Shimadzu EDX 7000 Energy Dispersive X-ray Fluorescence Spectrometer (Shimadzu Scientific Instruments, Japan) with the high-performance silicon drive detector and a high level of sensitivity. The high-performance BET analyzer model of NOVA touch 2LX (Quantachrome Instruments, USA) was employed to characterize the surface area and pore volume. The catalyst structure was analyzed using SEM Jeol JSM-IT200 (JEOL GmbH, Germany) with high-resolution imaging in HV/LV/SE/BSE and 5x–300,000x magnifications.

2.4 WGSR Experiment

The catalytic activity of the WGSR process was performed using a micro-activity flow reactor system. It has a 9 mm internal

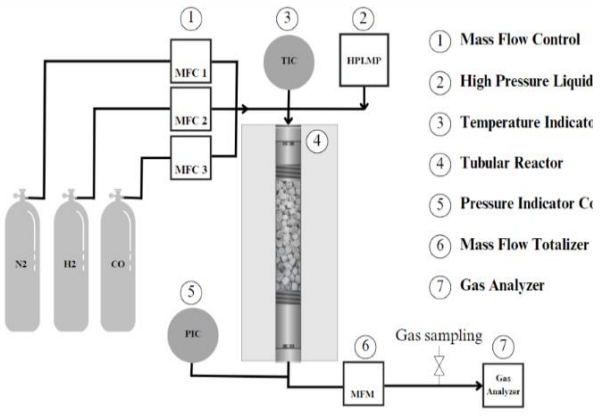

Fig. 2 Experimental apparatus.

diameter, a 14.5 mm external diameter, and a 305 mm length and was made of SUS-316L stainless steel. Furthermore, it is equipped with measured and controlled parameters, including steam and gas flow rate, reactor temperature, and pressure. The system ensured the absence of gas leaks. A schematic representation of the experimental apparatus is illustrated in Figure 2.

The WGSR process in a micro-activity flow reactor system consists of several key steps: preheating, reduction, preheating 2, reaction, nitrogen flush, and cooling. Each run required 2.0 g of catalyst inserted into the tubular reactor. The reactor was progressively preheated to 200 °C with a heating rate of 10 °C per minute. Traces of trapped air were removed by flowing nitrogen at 150 mL/min for 10 minutes. The catalyst was reduced for 60 minutes at 200 °C with hydrogen gas at 30 mL/min. Afterward, the reactor was purged with 150 mL/min of nitrogen to remove the residual hydrogen. The reactor was further heated to 250 °C before the start of the reaction to remove the residual hydrogen. CO gas with a 200 mL/min flow rate and steam (H_2O) was then introduced into the reactor with a steam-to-CO ratio of 3:1.

The reaction was carried out at 250 °C for 30 minutes. The temperature was maintained, and the flow rate ratio was continually and steadily controlled. The gas product composition was measured using a Gasboard 3100P gas analyzer. The CO conversion was determined using the formula illustrated in Equation (2) (Li *et al.* 2014).

$$X_{CO}(\%) = \frac{C_{H_2}}{C_{H_2}+C_{CO}} \times 100\% \quad (2)$$

X_{CO} represented the conversion of carbon monoxide. The H_2 and CO concentrations in the product gas were represented by C_{H2} and $C_{CO,}$ respectively.

3. Results and Discussion

3.1 Catalyst Characteristics

presents the metal composition of the commercial and synthesized catalysts based on the EDX result. CZA-431, CZA-531, and CZA-631 had a Cu percentage of 49.44%, 55.84%, and 62.18%, respectively. The Cu content was proportional to the molarity of the Cu solution in the catalyst precursors preparation step, which were 4 M, 5 M, and 6 M for CZA-431, CZA-531, and CZA-631, respectively. CZA-431 had the closest Cu:Zn:Al composition (49.44%: 41.74%: 8.82%) to the CZA-SC metal composition (41.61%: 49.01%: 9.38%). The impact of the metal composition on catalyst performance will be discussed in the discussion on catalyst performance results.

Table 1
The composition of metals from EDX results

Catalyst	Metal composition		
	Cu (%)	Zn (%)	Al (%)
CZA-SC	41.61	49.01	9.38
CZA-431	49.44	41.74	8.82
CZA-531	55.84	37.10	7.06
CZA-631	62.18	32.52	5.31

CuO, ZnO, and Al_2O_3 metal oxides are vital in CZA catalyst activity. Since the EDX result alone could not present the existence of the metal oxides mentioned above, XRD analysis was conducted to find the oxide phase of each metal observed in the EDX result. The XRD patterns of the CZA catalysts are displayed in Fig. .

The CuO and ZnO oxide phases exhibited characteristic peak patterns in the 30° to 70° range. The intensity of the reflections associated with Cu becomes more prominent as the Cu content increases. However, the intensity of CuO and ZnO peaks in synthesized catalysts was still below the CZA-SC catalyst, suggesting that the amount of CuO and ZnO crystals in synthesized catalysts was fewer than in commercial ones. The typical CuO reflections were rather broad in all catalysts, indicating an unclear crystalline phase and likely overlapping with broad ZnO reflections. These broad reflections also suggest that the crystal size of both ZnO and CuO was relatively small (Ereña *et al.* 2003). Notably, no peaks associated with alumina were observed, indicating the amorphous nature of this low-concentration promoter.

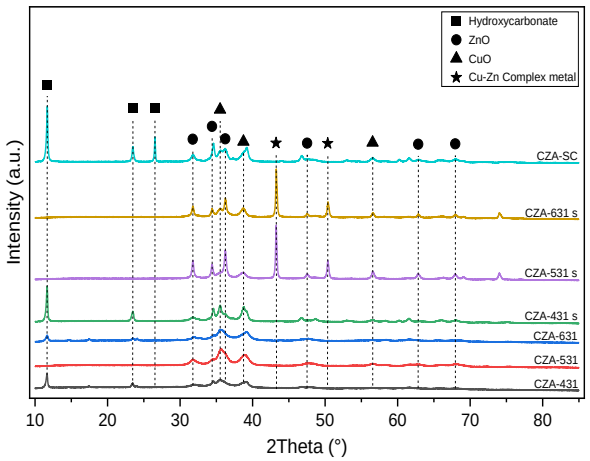

Fig. 3. The diffractogram pattern of CZA-SC, CZA-431, CZA-531, and CZA-631 fresh and spent catalyst (s)

Table 2
The CZA catalyst characteristics

Catalyst	Pore Volume (cm^3/g)	Surface Area (m^2/g)
CZA-431	0.3165	76.88
CZA-531	0.2242	60.53
CZA-631	0.1868	53.64

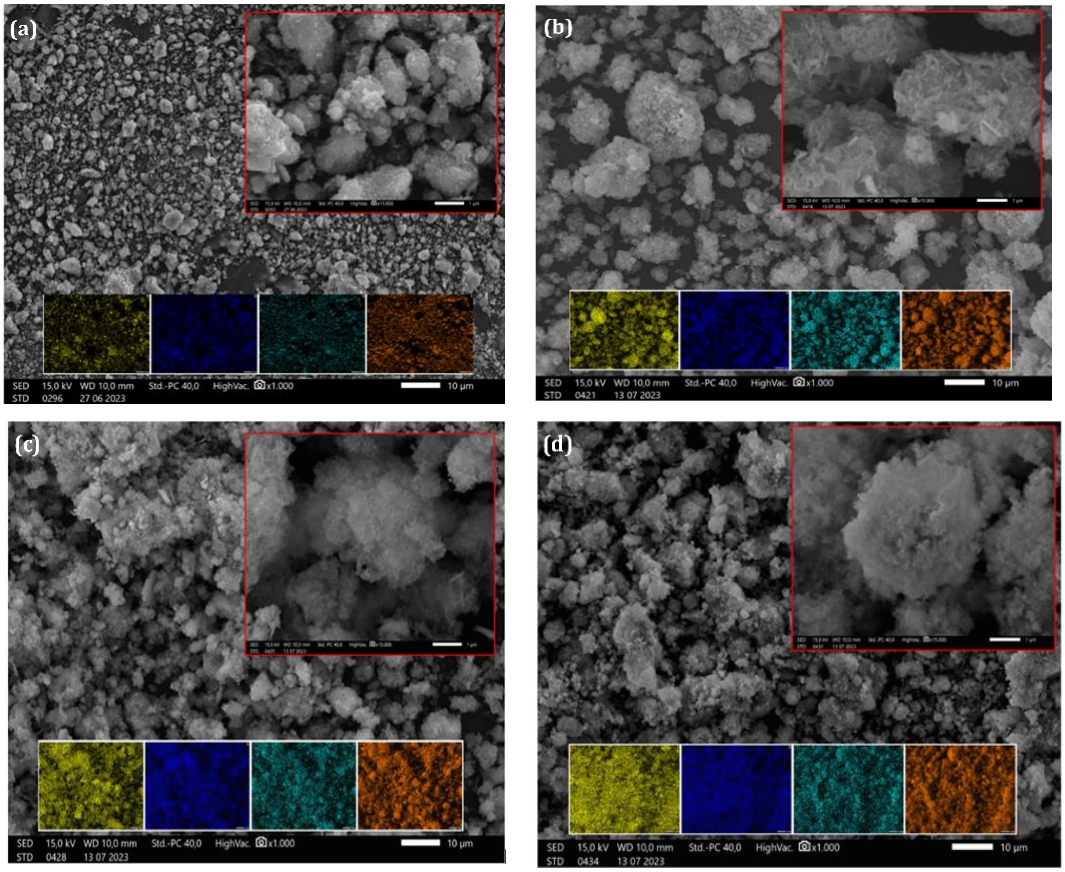

Fig. 4 Catalyst structure from SEM results for (a) CZA-SC, (b) CZA-431, (c) CZA-531, and (d) CZA-631.

Along with CuO and ZnO phases, other peaks were observed in the 10–11° and 23–24° range. Those peaks were very intense in the CZA-SC, followed by CZA-431, which showed the highest peaks among the synthesized CZA. Those peaks corresponded to the hydrotalcite analog compound ($Cu_xZn_{(6-x)}Al_2(OH)_{16}CO_3{\cdot}4H_2O$) (Kowalik *et al.* 2019), which were identified as residual hydroxy carbonates existed in the CZA catalyst. This residual hydroxycarbonate was believed to enhance the catalyst activity due to its ability to form highly active sites (Baltes, Vukojević, & Schüth 2008) and ensuing production of copper suboxide species (Plyasova *et al.* 1995). The existence of residual carbonates likely delayed the catalyst structure's fragmentation before reducing the copper species and forming more petite, more interactive particles (Baltes, Vukojević, & Schüth 2008).

The spent catalysts of the synthesized CZA catalyst were also analysed, and the results were displayed in the diffractogram pattern as CZA-431-s, CZA-531-s, and CZA-631-s. Several new peaks appeared in the 40-45° and 50° range for both CZA-531-s and CZA-631-s catalysts. These peaks were related to Cu-Zn complex metal ($Cu_{0.951}Zn_{0.049}$). Since this complex metal is only found in the catalyst with a higher content of Cu, it might correlate with the closer distance between Cu particles that promoted the metal complex formation with the Zn nearby during the reaction. The narrow reflections of the peaks indicated the big crystal size of this metal complex. Along with the formation of the Cu-Zn metal complex, it can be observed that ZnO peaks get narrower reflections compared to the fresh catalyst, which could indicate the growth of ZnO crystal, which further will affect the catalyst activity.

Surface characteristics, including surface area and pore volume, were crucial for the catalyst since the active site needed for the reaction was distributed on the surface area. The higher surface area will theoretically result in higher catalytic activity (Bernard *et al.* 2021). The surface characteristics of the CZA catalysts are presented in Table 2. The CZA-431 catalyst had the highest pore volume and surface area, followed by CZA-531 and CZA-631 catalysts.

Both pore volume and surface area decreased along with increased Cu content, which may correlate with decreased Al content. The specific surface area in the catalyst was known to be strongly affected by Al_2O_3 contents, which act as textural promoters or spacers between Cu active sites (Ahn *et al.* 2020). The higher the Al content in the catalyst, the wider the distance between Cu particles. Therefore, the Cu/Al ratio will inversely relate to the specific surface area. In this study, CZA-431, CZA-531, and CZA-631 have a Cu/Al ratio of 5.61, 7.91, and 11.71, respectively. CZA-431 had the lowest Cu/Al ratio of 5.61, giving the highest specific surface area of 76.88 m^2/g. However, CZA-SC had a lower specific surface area than the synthesized catalysts, even though it had a lower Cu/Al ratio than the CZA-431 catalyst. It may correlate with the hydroxycarbonate content in the CZA-SC catalyst. The narrow reflections of the hydroxycarbonate peaks indicate this compound's big crystal size, which may reduce the specific surface area of the CZA-SC catalyst. Cu concentration affects the catalyst's surface area as well. A high Cu content prevents the opening of pores, resulting in a decrease in the catalyst's surface area. This finding is consistent with the report by Lucarelli *et al.* (2018).

The structure of the catalyst is also essential to be discovered as it displays the catalyst particle's form, condition, and dispersion. The structure of the catalyst can be characterized using SEM. Figure 4 shows the SEM results for this research's commercial and synthesized catalysts. The Catalyst structure for CZA-SC, CZA-431, CZA-531, and CZA-631 are depicted in Figure 4(a), 4(b), 4(c), 4(d), respectively. The metal dispersion from the EDX result is mapped as yellow, blue, turquoise, and orange for Cu, Zn, Al, and O, respectively.

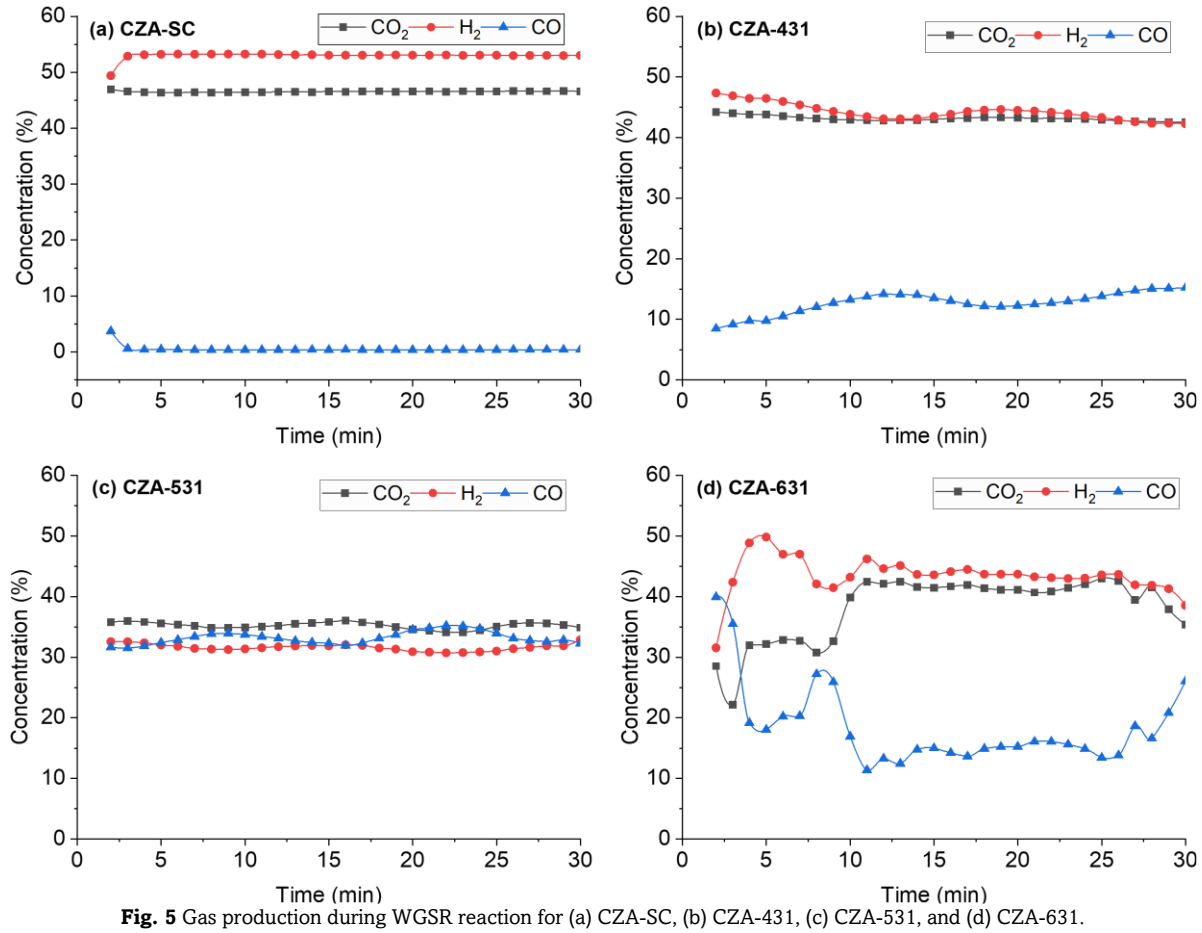

Fig. 5 Gas production during WGSR reaction for (a) CZA-SC, (b) CZA-431, (c) CZA-531, and (d) CZA-631.

The catalyst particles were found to be in an almost good spherical form for all Cu, Zn, and Al particles, as seen in the SEM images. The wider distance between Cu particles, decreased Cu/Al ratio, or increased Al content was also confirmed. The investigation reveals that CZA-431, CZA-531, and CZA-631 exhibit Cu/Al ratios of 5.61, 7.91, and 11.71, respectively. It indicates a higher concentration and denser distribution of Cu, as depicted in Figure 4(a), 4(b), 4(c), and 4(d). The CZA-431 sample had the lowest Cu/Al ratio of 5.61, indicating a slightly lower Cu density, as shown in Figure 4(b).

Furthermore, the presence of Zn content acted as an inhibitor of Cu aggregation, reducing the size of Cu particles (Ye *et al.* 2023). The CZA-631 catalyst has the most excellent Cu/Al ratio of 5.61, indicating that the particle spacing in the catalyst is relatively close. The particles even stick together, forming some aggregates, as seen in Figure 4(d). This is due to the low Al and Zn concentration in the catalyst. The variance in catalyst particle size and dispersion may be attributed to differences in the catalyst's production and preparation processes. The preparation methods impact the physicochemical characteristics of catalysts, including active metal dispersion, specific surface area, reducibility, and crystallite size, which ultimately affect the catalytic performance despite identical loading (Shim *et al.* 2016).

3.2 WGSR on CZA Catalysts

The WGSR catalyst's performance can be determined by testing it in the reaction and comparing the influence of the catalyst in the reaction by plotting the gas concentration during the reaction. WGSR can be represented as Equation (1), where H_2 production is expected, and more H_2 production is preferred.

Figure 5 shows the CO, CO_2, and H_2 gas concentrations during the WGSR reaction. The hydrogen, CO_2, and CO gas concentrations produced in the reaction utilizing the CZA-SC catalyst were relatively stable, and the stable condition was obtained 3 minutes after the reaction began, see Figure 5(a). This condition is also proper for reactions using CZA-431 and CZA-531 catalysts, as illustrated in Figure 5 (b) and 5(c). However, the gas concentration in the reaction using the CZA-631 catalyst still fluctuated until 10 minutes after the reaction, as shown in Figure 5(d). After 10 minutes of reaction, the concentration of gas produced remained stable until 27 minutes, then decreased until the end of the reaction. This fluctuation of the gas produced can be related to the Cu content in the catalyst. The Cu content of the CZA-631 catalyst was 62.18%, the highest among the other synthesized catalysts. Hypothetically, the increase in Cu content should increase the catalyst activity as it functions as the active site in the catalysts. A higher Cu content of up to 8% can increase the catalyst surface area, resulting in higher activity (Gradisher, Dutcher, & Fan 2015). The quantity of Cu° active sites is related to H_2 generation. The formation of 1 mol H_2 indicated that the 2 Cu° active site is oxidized to be Cu^+ (Taniya *et al.* 2023). However, in this research, the results suggest that the difference in Cu concentration in CZA-431 and CZA-631 catalysts resulted in almost the same concentration of H_2 production, and on CZA-531, the H_2 production was even lower.

The average H_2 gas concentration obtained from the reaction using the CZA-SC catalyst was 53%, as shown in Table 3. While on the reactions using CZA-431, 531, and 631 catalysts, the average H_2 gas production was lower, i.e., 44.06%, 31.59%, and 43.86%, respectively. Considering CO conversion, the

Table 3
The average H_2 production and CO conversion during WGSR by CZA catalyst

Catalyst	Average H_2 Concentration (%)	CO Conversion (%)
CZA-SC	53.00	99.28
CZA-431	44.06	77.44
CZA-531	31.59	48.75
CZA-631	43.86	71.67

highest hydrogen content was obtained from the CZA-SC catalyst reaction, reaching 99.28%. In contrast, for CZA-431, CZA-531, and CZA-631, the CO conversion reached 77.44%, 48.75 %, and 71.67% respectively. In this study, the CO conversion decreases when the Cu content increases. The decrease in CO conversion on CZA-531 and CZA-631 catalysts is due to more significant amounts of Cu that tend to form Cu-Zn complex metal ($Cu_{0.951}Zn_{0.049}$) as found in the XRD photo shown in Fig. . This complex metal affects reaction stability, as seen in CZA-531 and CZA-631. The conversion is also affected by the Zn content, which in this case is determined by the ratio of Cu/Zn (Reddy & Smirniotis 2015). The Cu/Zn ratios for CZA-431, CZA-531, and CZA-631 are 0.89, 1.18, 1.51, and 1.91, respectively. CZA-431, which has a Cu/Zn ratio of 1.18 and is similar in Cu/Zn ratio to CZA-SC at 0.85, resulted in higher conversion rates than CZA-531 and CZA-631. Meza Fuentes *et al.* (2021) reported that a Cu/Zn ratio of 1M was more efficient than materials with higher copper content.

Meanwhile, the hydrogen yield obtained from CZA-631 is similar to CZA-431 with unstable product distribution. Conversely, the hydrogen content yield and conversion of CZA-531 was low due to hydroxycarbonate in the CZA-431 and CZA-631 synthesized catalysts. However, this hydroxycarbonate was not found in the CZA-531, as discussed in the catalyst characterization chapter. Meanwhile, Cu-Zn complex metal ($Cu_{0.951}Zn_{0.049}$) was not found in CZA-431 and CZA-SC catalysts. This complex compound can contribute to reducing catalyst activity. Moreover, the Al content as a structural promoter cannot compensate for the high Cu content, resulting in the low dispersion of the catalyst particles (Zhang *et al.* 2018).

3.3 WGSR on CZA-CaO catalysts

Based on the catalytic testing data for the WGSR, the synthesized catalysts needed improvements to match the performance of commercial catalysts. The catalyst could be refined by changing the support or structure of the catalyst and adding some promoters to the catalyst (Desgagnés, Alizadeh Sahraei, & Iliuta 2023; García-Moncada *et al.* 2022). Adding promoters improves reaction activity while increasing the catalyst-specific surface area inhibits precipitation on the modified catalyst's surface and improves performance (Song *et al.* 2016). The improvement done in this research was the use of CaO to increase the hydrogen gas content.

Figure 6 shows the gas product concentration of the WGSR process using the CZA catalysts with the addition of CaO. With the addition of CaO, each synthesized catalyst improved its hydrogen production performance to 52.03%, 51.15%, and 46.46%, respectively, as illustrated in Figure 6 (a), 6(b), and 6(c), respectively. The performance of CZA-431 came close to that of WGS-SC (53%). With the addition of CaO, CZA-631 also reached the exothermic equilibrium faster than without CaO. Faster gas production stability was manifested by the augmented CZA-631 with CaO in just 3 minutes compared with CZA-631 without CaO in 10 minutes, as shown in Fig 5(d) and

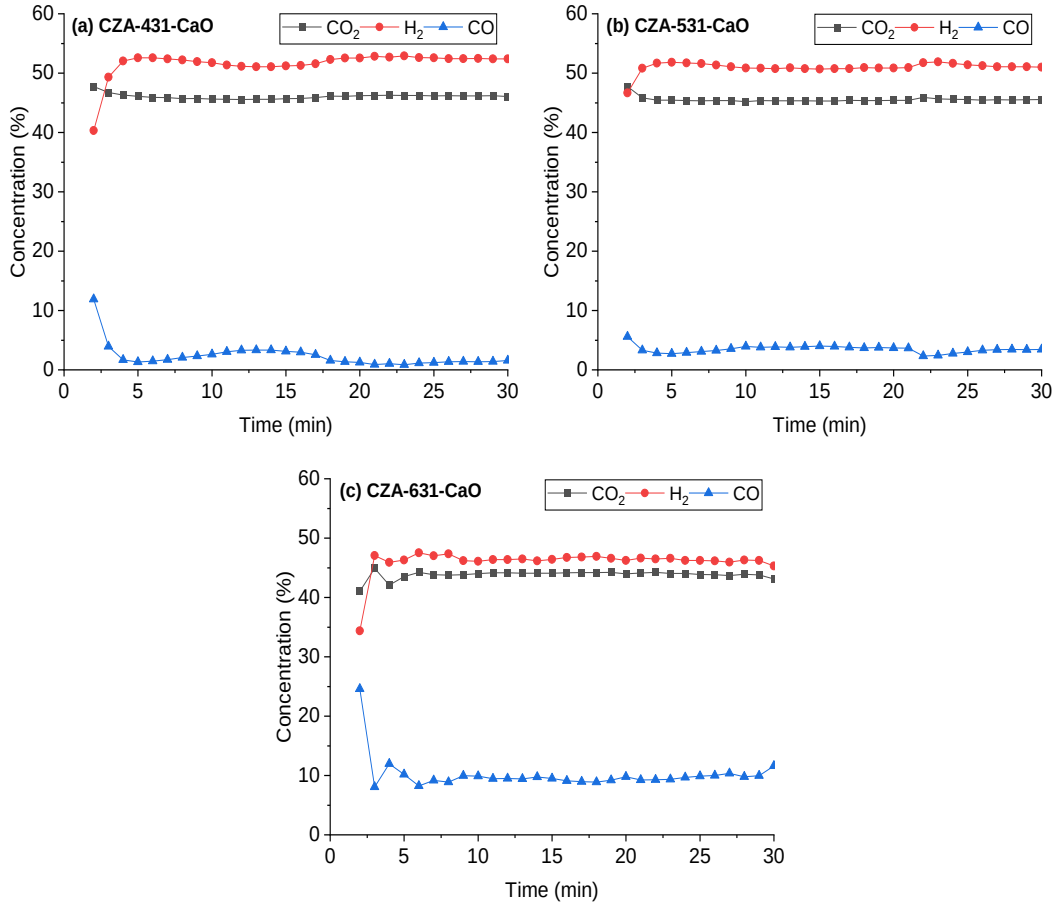

Fig. 6 The hydrogen production under CZA-SC, synthesized CZA, and CaO-added CZA catalyst

Table 4
The gas production improvement under the effect of CaO addition to the CZA catalyst

Catalyst	CO		H_2	
	Conversion (%)	Improvement (%)	Average Concentration (%)	Improvement (%)
CZA-431-CaO	97.39	+ 24.42	52.03	+ 18.09
CZA-531-CaO	96.71	+ 92.37	51.15	+ 61.93
CZA-631-CaO	95.41	+ 15.63	46.46	+ 5.92

Figure 6(c), which can be attributed to the role of CaO. Adding CaO reduces metal particle size, enhances the anti-sintering properties of the active metal, and confirms the stability of the catalyst (Mo *et al.* 2019). Moreover, the CaO confinement effect would give additional active sites and improve CO_2 adsorption (Sengupta & Deo 2015). It explains why the CZA catalyst performs better when CaO is added to the WGSR process.

CaO addition in CZA-531 exhibits tremendous effects regarding hydrogen gas concentration and CO conversion. The hydrogen gas concentration improved from 31.59% to 51.15% (61.93%), and CO conversion jumped from 48.75% to 93.78% (92.37%), as depicted in Table 4. CO_2, H_2, and CO gas conversions surged due to CaO addition. Overall, the increase in gas product quality and CO conversion indicates that CaO positively affects the WGSR process, as seen in Table 4. Even though the CaO can be a CO_2 absorber to produce $CaCO_3$ according to the chemical reaction in Equation (3), as shown in Figure 7, $CaCO_3$ appears with very little intensity. However, this reaction can only occur at temperatures higher than WGSR (250 °C). CaO can also adsorb the CO_2 produced in the reaction, allowing the reaction equilibrium to shift toward the products (Günter *et al.* 2001). Besides, CaO can also react with H_2O in the feed to form $Ca(OH)_2$, as shown in the chemical reaction in Equation (4) (El Bazi *et al.* 2022). Li, Liu and Cai (2012) reported that CaO was converted to $Ca(OH)_2$ in 0% of the steam volume at a temperature of 250 °C (Li, Liu, & Cai 2012). $CaCO_3$ emerged in CZA-431, while $Ca(OH)_2$ appeared in all CZA-431, CZA-531 and CZA-631. On the other hand, $CaCO_3$ is also seen in the diffractogram in Figure 7 but with a small intensity.

$$CaO + CO_2 \leftrightarrow CaCO_3 \quad (3)$$

$$CaO + H_2O \leftrightarrow Ca(OH)_2 \quad (4)$$

The role of CaO in increasing H_2 production can be attributed to dissociating H_2O since this is the step that limits the rate of the WGSR process (Figueiredo *et al.* 1998; Yan *et al.* 2021). CaO can also adsorb the CO_2 produced in the reaction, allowing the reaction equilibrium to shift toward the products (Günter *et al.* 2001). The existence of CaO can also reduce the metal's particle size by improving the active metal's anti-sintering properties (Mo *et al.* 2019; Hadiyanto *et al* 2016). Furthermore, the CaO confinement effect would give additional active sites and improve CO_2 adsorption (Sengupta & Deo 2015). In this study, CaO addition to the CZA catalyst has significantly improved H_2 gas production.

Moreover, adding CaO resulted in a more stable reaction process that practically corresponded to the commercial catalyst. The WGSR progresses on the surface of CaO through the redox-a route, wherein H_2O decomposes into hydroxyl and atomic hydrogen, followed by hydroxyl dissociation and CO oxidation by atomic oxygen. The CaO surface allows H_2O to spontaneously dissociate, which acts as the rate-determining step for the WGSR. The presence of CaO diminishes the energy barrier for the production of CO_2 during the WGSR. Essentially, our research involved introducing CaO to the CuZnAl synthesis catalyst. It led to a change favoring higher hydrogen production in the WGSR reaction, improving conversion performance.

Based on the results from this study, the addition of CaO on CZA catalyst in WGSR can also be employed to convert biomass feedstock to produce renewable energy, such as biohydrogen or hydrogen-rich syngas, primarily through the gasification process- WGSR. However, some constraints and challenges must be faced, such as the gas separation process and the high energy required to produce steam. In addition, the CO_2 composition of the gas product is still relatively high. Thus, in future studies, a suitable catalyst design, kinetics of the WGSR, optimization of the process parameters, and economical feasibility analysis are needed to overcome these challenges. Tleubergenova, Han and Meng (2024) stated that gasification technology is under TRL (Technology Readiness Level) 7 and will be TRL 9 in the next 20-30 years. Thus, hydrogen production using green technology and renewable energy sources for large-scale industrial production has recently gained worldwide attention.

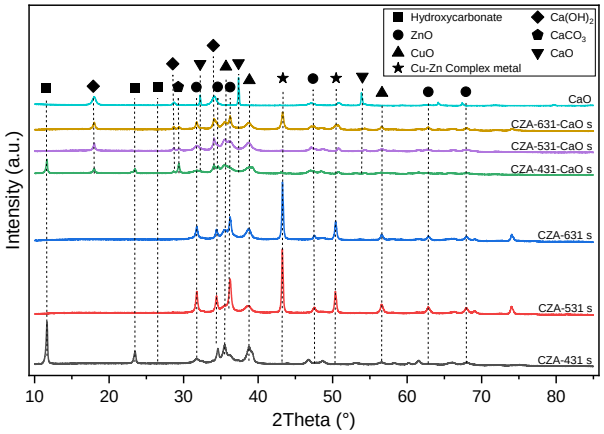

Fig. 7 The diffractogram pattern of CaO-CZA Catalyst fresh and spent catalyst (s)

4. Conclusion

This research synthesized CZA catalysts using the co-precipitation method at various Cu:Zn:Al molar ratios. Applied to WGSR, the CZA-431 catalyst (4:3:1) generated the highest H_2 content in the gas product with a CO conversion of 77.44%. CZA-531 and CZA-631 catalysts had higher Cu concentrations, of which the excess tended to promote the formation of the Cu-Zn metal complex, affecting the catalyst activity. This performance of CZA-431 was still not comparable to that of the commercial catalyst CZA-SC, with a CO conversion of 99.28%. To boost the H_2 production, CaO was added to the synthesized CZA catalyst. CaO was known to have surfaces that enabled instantaneous H_2O dissociation, which was the controlling step in WGSR. Adding CaO to the CZA-431 catalyst improved the CO conversion to 97.39%. CaO addition to the CZA catalyst effectively increased the H_2 gas production. It accelerated the exothermic equilibrium of WGSR, leading to the stability of gas product composition. The ability of the CaO-CZA-431 catalyst

to convert CO to produce H_2 is encouraging, and it can be the answer to the challenge in the biohydrogen production process via the thermal route.

This work can be utilized in future research to explore the application of thermochemical conversion processes in biomass gasification technology. The focus would be on using renewable resources to produce hydrogen, which can be used as an energy source.

Acknowledgements

This research was supported by the National Research and Innovation Agency (BRIN), specifically the Advanced Characterization Laboratory - Serpong (Physics), for providing the resources needed to conduct the BET analysis, XRD, and SEM energy-dispersive X-ray fluorescence experiments described here.

Author Contributions: A.S.: supervision, project administration, review and editing E.R.: conceptualization, methodology, F.R.S.: visualization, resources, H.N.A.: writing—original draft, I.M.: conceiving and planning the experiments, formal analysis, N.R.: synthesizing and characterizing the catalyst, T.P.R: collecting sample, characterizing, and analyzing, T.A. and W.P.: performing the experiments, collecting data, Z.D.H.: writing—review and editing, performing analytical calculation, validation.

Funding: The New Energy and Industrial Technology Development Organization of Japan (NEDO) supported this research in partnership with the National Research and Innovation Agency (BRIN).

Conflicts of Interest: none

References

Acharya, B., Dutta, A., & Basu, P. (2010). An investigation into steam gasification of biomass for hydrogen enriched gas production in presence of CaO. *International Journal of Hydrogen Energy*, *35*(4), 1582-1589; https://doi.org/10.1016/j.ijhydene.2009.11.109

Agaton, C. B., Batac, K. I. T., & Reyes Jr, E. M. (2022). Prospects and challenges for green hydrogen production and utilization in the Philippines. *International Journal of Hydrogen Energy*, *47*(41), 17859-17870; https://doi.org/10.1016/j.ijhydene.2022.04.101

Ahn, S.-Y., Na, H.-S., Jeon, K.-W., Lee, Y.-L., Kim, K.-J., Shim, J.-O., & Roh, H.-S. (2020). Effect of Cu/CeO2 catalyst preparation methods on their characteristics for low temperature water−gas shift reaction: A detailed study. *Catalysis Today*, *352*, 166-174; https://doi.org/10.1016/j.cattod.2019.11.017

Al-Baghdadi, M. A. R. S., Ahmed, S. S., & Ghyadh, N. A. (2023). Three-dimensional CFD-solid mechanics analysis of the hydrogen internal combustion engine piston subjected to thermomechanical loads [Hydrogen fuel; Internal combustion engines; Piston; Thermomechanical loads; CFD]. *International Journal of Renewable Energy Development*, *12*(3), 9; https://doi.org/10.14710/ijred.2023.52496

Arregi, A., Amutio, M., Lopez, G., Bilbao, J., & Olazar, M. (2018). Evaluation of thermochemical routes for hydrogen production from biomass: A review. *Energy Conversion and Management*, *165*, 696-719; https://doi.org/10.1016/j.enconman.2018.03.089

Aziz, M., Darmawan, A., & Juangsa, F. B. (2021). Hydrogen production from biomasses and wastes: A technological review. *International Journal of Hydrogen Energy*, *46*(68), 33756-33781; https://doi.org/10.1016/j.ijhydene.2021.07.189

Baltes, C., Vukojević, S., & Schüth, F. (2008). Correlations between synthesis, precursor, and catalyst structure and activity of a large set of CuO/ZnO/Al2O3 catalysts for methanol synthesis. *Journal of Catalysis*, *258*(2), 334-344; https://doi.org/10.1016/j.jcat.2008.07.004

Baraj, E., Ciahotný, K., & Hlinčík, T. (2021). The water gas shift reaction: Catalysts and reaction mechanism. *Fuel*, *288*, 119817; https://doi.org/10.1016/j.fuel.2020.119817

Bernard, P., Stelmachowski, P., Broś, P., Makowski, W., & Kotarba, A. (2021). Demonstration of the Influence of Specific Surface Area on Reaction Rate in Heterogeneous Catalysis. *Journal of Chemical Education*, *98*(3), 935-940; https://doi.org/10.1021/acs.jchemed.0c01101

Chen, H.-B., Liao, D.-W., Yu, L.-J., Lin, Y.-J., Yi, J., Zhang, H.-B., & Tsai, K.-R. (1999). Influence of trivalent metal ions on the surface structure of a copper-based catalyst for methanol synthesis. *Applied Surface Science*, *147*(1), 85-93; https://doi.org/10.1016/S0169-4332(99)00081-1

Chen, W., Li, T., Ren, Y., Wang, J., Chen, H., & Wang, Q. (2023). Biological hydrogen with industrial potential: Improvement and prospection in biohydrogen production. *Journal of Cleaner Production*, *387*, 135777; https://doi.org/10.1016/j.jclepro.2022.135777

Damayanti, A., Sarto, S., & Sediawan, W. B. (2020). Biohydrogen Production by Reusing Immobilized Mixed Culture in Batch System [biohydrogen; reused beads; immobilization; mixed culture; batch]. *2020*, *9*(1), 6; https://doi.org/10.14710/ijred.9.1.37-42

Dasireddy, V. D. B. C., Rubin, K., Pohar, A., & Likozar, B. (2020). Surface structure–activity relationships of Cu/ZnGaOX catalysts in low temperature water–gas shift (WGS) reaction for production of hydrogen fuel. *Arabian Journal of Chemistry*, *13*(4), 5060-5074; https://doi.org/10.1016/j.arabjc.2020.02.005

Dawood, F., Anda, M., & Shafiullah, G. M. (2020). Hydrogen production for energy: An overview. *International Journal of Hydrogen Energy*, *45*(7), 3847-3869; https://doi.org/10.1016/j.ijhydene.2019.12.059

Desgagnés, A., Alizadeh Sahraei, O., & Iliuta, M. C. (2023). Improvement strategies for Ni-based alcohol steam reforming catalysts. *Journal of Energy Chemistry*, *86*, 447-479; https://doi.org/10.1016/j.jechem.2023.07.011

Dou, B., Zhang, H., Song, Y., Zhao, L., Jiang, B., He, M., Ruan, C., Chen, H., & Xu, Y. (2019). Hydrogen production from the thermochemical conversion of biomass: issues and challenges [10.1039/C8SE00535D]. *Sustainable Energy & Fuels*, *3*(2), 314-342; https://doi.org/10.1039/C8SE00535D

Duman, G., & Yanik, J. (2017). Two-step steam pyrolysis of biomass for hydrogen production. *International Journal of Hydrogen Energy*, *42*(27), 17000-17008; https://doi.org/10.1016/j.ijhydene.2017.05.227

El Bazi, W., Bideq, M., Abidi, A., Said, Y., & Bajil, O. (2022). Numerical Study of a Water Gas Shift Fixed Bed Reactor Operating at Low Pressures. *Bulletin of Chemical Reaction Engineering and Catalysis*, 17 (2), 304-321. https://doi.org/10.9767/bcrec.17.2.13510.304-321

Ereña, J., Arandes, J. M., Garoña, R., Gayubo, A. G., & Bilbao, J. (2003). Study of the preparation and composition of the metallic function for the selective hydrogenation of CO2 to gasoline over bifunctional catalysts. *Journal of Chemical Technology & Biotechnology*, *78*(2-3), 161-166; https://doi.org/10.1002/jctb.720

Fajín, J. L. C., & Cordeiro, M. N. D. S. (2021). Insights into the catalytic activity of trimetallic Al/Zn/Cu surfaces for the water gas shift reaction. *Applied Surface Science*, *542*, 148589; https://doi.org/10.1016/j.apsusc.2020.148589

Figueiredo, R. T., Martínez-Arias, A., Granados, M. L., & Fierro, J. L. G. (1998). Spectroscopic Evidence of Cu–Al Interactions in Cu–Zn–Al Mixed Oxide Catalysts Used in CO Hydrogenation. *Journal of Catalysis*, *178*(1), 146-152; https://doi.org/10.1006/jcat.1998.2106

García-Moncada, N., Jurado, L., Martínez-Tejada, L. M., Romero-Sarria, F., & Odriozola, J. A. (2022). Boosting water activation determining-step in WGS reaction on structured catalyst by Mo-doping. *Catalysis Today*, *383*, 193-204; https://doi.org/10.1016/j.cattod.2020.06.003

Ghodke, P. K., Sharma, A. K., Jayaseelan, A., & Gopinath, K. P. (2023). Hydrogen-rich syngas production from the lignocellulosic biomass by catalytic gasification: A state of art review on advance technologies, economic challenges, and future prospectus. *Fuel*, *342*, 127800; https://doi.org/10.1016/j.fuel.2023.127800

Gogate, M. (2020). Water-Gas Shift Reaction: Advances and Industrial Applications. *Progress in Petrochemical Science*, *3*; https://doi.org/10.31031/PPS.2020.03.000569

Gradisher, L., Dutcher, B., & Fan, M. (2015). Catalytic hydrogen production from fossil fuels via the water gas shift reaction. *Applied Energy*, *139*, 335-349; https://doi.org/10.1016/j.apenergy.2014.10.080

Gunawardana, P. V. D. S., Lee, H. C., & Kim, D. H. (2009). Performance of copper–ceria catalysts for water gas shift reaction in medium temperature range. *International Journal of Hydrogen Energy*, *34*(3), 1336-1341; https://doi.org/10.1016/j.ijhydene.2008.11.041

Günter, M. M., Ressler, T., Bems, B., Büscher, C., Genger, T., Hinrichsen, O., Muhler, M., & Schlögl, R. (2001). Implication of the microstructure of binary Cu/ZnO catalysts for their catalytic activity in methanol synthesis. *Catalysis Letters*, *71*(1), 37-44; https://doi.org/10.1023/A:1016696022840

Hadiyanto, H., Lestari, S.P., Abdullah, A., Widayat, W., Sutanto, H. (2016). The development of fly ash-supported CaO derived from mollusk shell of Anadara granosa and Paphia undulata as heterogeneous CaO catalyst in biodiesel synthesis. *Int J Energy Environ Eng* 7, 297–305. https://doi.org/10.1007/s40095-016-0212-6

Havilah, P. R., Sharma, A. K., Govindasamy, G., Matsakas, L., & Patel, A. (2022). Biomass Gasification in Downdraft Gasifiers: A Technical Review on Production, Up-Gradation and Application of Synthesis Gas. *Energies*, *15*(11), 3938; https://www.mdpi.com/1996-1073/15/11/3938

He, Y., Tu, J., Li, D., Lin, C., Mo, Z., Huang, S., Hu, C., Shen, D., & Wang, T. (2023). Investigation of hydrogen-rich syngas production from biomass gasification with CaO and steam based on real-time gas release behaviors. *Journal of Analytical and Applied Pyrolysis*, *169*, 105851; https://doi.org/10.1016/j.jaap.2022.105851

Heidenreich, S., & Foscolo, P. U. (2015). New concepts in biomass gasification. *Progress in Energy and Combustion Science*, *46*, 72-95; https://doi.org/10.1016/j.pecs.2014.06.002

Huber, G. W., Iborra, S., & Corma, A. (2006). Synthesis of Transportation Fuels from Biomass: Chemistry, Catalysts, and Engineering. *Chemical Reviews*, *106*(9), 4044-4098; https://doi.org/10.1021/cr068360d

Jang, W.-J., Shim, J.-O., Jeon, K.-W., Na, H.-S., Kim, H.-M., Lee, Y.-L., Roh, H.-S., & Jeong, D.-W. (2019). Design and scale-up of a Cr-free Fe-Al-Cu catalyst for hydrogen production from waste-derived synthesis gas. *Applied Catalysis B: Environmental*, *249*, 72-81; https://doi.org/10.1016/j.apcatb.2019.02.036

Kalinci, Y., Hepbasli, A., & Dincer, I. (2009). Biomass-based hydrogen production: A review and analysis. *International Journal of Hydrogen Energy*, *34*(21), 8799-8817; https://doi.org/10.1016/j.ijhydene.2009.08.078

Kowalik, P., Wiercioch, P., Bicki, R., Próchniak, W., Antoniak-Jurak, K., Michalska, K., & Słowik, G. (2019). Flash-Calcined CuZnAl-LDH as High-Activity LT-WGS Catalyst. *European Journal of Inorganic Chemistry*, *2019*(13), 1792-1798; https://doi.org/10.1002/ejic.201801553

Lanjekar, P. R., Panwar, N. L., & Agrawal, C. (2023). A comprehensive review on hydrogen production through thermochemical conversion of biomass for energy security. *Bioresource Technology Reports*, *21*, 101293; https://doi.org/10.1016/j.biteb.2022.101293

Lepage, T., Kammoun, M., Schmetz, Q., & Richel, A. (2021). Biomass-to-hydrogen: A review of main routes production, processes evaluation and techno-economical assessment. *Biomass and Bioenergy*, *144*, 105920; https://doi.org/10.1016/j.biombioe.2020.105920

Li, B., Wei, L., Yang, H., Wang, X., & Chen, H. (2014). The enhancing mechanism of calcium oxide on water gas shift reaction for hydrogen production. *Energy*, *68*, 248-254; https://doi.org/10.1016/j.energy.2014.02.088

Li, Z., Liu, Y., & Cai, N. (2012). Effect of CaO hydration and carbonation on the hydrogen production from sorption enhanced water gas shift reaction. *International Journal of Hydrogen Energy*, *37*(15), 11227-11236; https://doi.org/10.1016/j.ijhydene.2012.04.160

Lucarelli, C., Molinari, C., Faure, R., Fornasari, G., Gary, D., Schiaroli, N., & Vaccari, A. (2018). Novel Cu-Zn-Al catalysts obtained from hydrotalcite-type precursors for middle-temperature water-gas shift applications. *Applied Clay Science*, *155*, 103-110; https://doi.org/10.1016/j.clay.2017.12.022

Martínez, I., Callén, M. S., Grasa, G., López, J. M., & Murillo, R. (2022). Sorption-enhanced gasification (SEG) of agroforestry residues: Influence of feedstock and main operating variables on product gas quality. *Fuel Processing Technology*, *226*, 107074; https://doi.org/10.1016/j.fuproc.2021.107074

Martínez, I., Kulakova, V., Grasa, G., & Murillo, R. (2020). Experimental investigation on sorption enhanced gasification (SEG) of biomass in a fluidized bed reactor for producing a tailored syngas. *Fuel*, *259*, 116252; https://doi.org/10.1016/j.fuel.2019.116252

Meza Fuentes, E., Rodríguez Ruiz, J., Massin, L., Cadete Santos Aires, F. J., da Costa Faro, A., Assaf, J. M., & Rangel, M. d. C. (2021). Characterization and performance within the WGS reaction of Cu catalysts obtained from hydrotalcites. *International Journal of Hydrogen Energy*, *46*(64), 32455-32470; https://doi.org/10.1016/j.ijhydene.2021.07.072

Mo, W., Ma, F., Ma, Y., & Fan, X. (2019). The optimization of Ni–Al2O3 catalyst with the addition of La2O3 for CO2–CH4 reforming to produce syngas. *International Journal of Hydrogen Energy*, *44*(45), 24510-24524; https://doi.org/10.1016/j.ijhydene.2019.07.204

Muharto, B., Saputro, F. R., Prabowo, W., Anggoro, T., Adiprabowo, A. B., Masfuri, I., & Irawan, B. B. (2023). Pyrolysis process control: temperature control design and application for optimum process operation. *International Journal of Electrical and Computer Engineering (IJECE)*, *14*, 1473-1485; https://doi.org/10.11591/ijece.v14i2.pp1473-1485

Na, H.-S., Ahn, S.-Y., Shim, J.-O., Jeon, K.-W., Kim, H.-M., Lee, Y.-L., Jang, W.-J., Jeon, B.-H., & Roh, H.-S. (2019). Effect of precipitation on physico-chemical and catalytic properties of Cu-Zn-Al catalyst for water-gas shift reaction. *Korean Journal of Chemical Engineering*, *36*(8), 1243-1248; https://doi.org/10.1007/s11814-019-0309-8

Nagar, R., Srivastava, S., Hudson, S. L., Amaya, S. L., Tanna, A., Sharma, M., Achayalingam, R., Sonkaria, S., Khare, V., & Srinivasan, S. S. (2023). Recent developments in state-of-the-art hydrogen energy technologies – Review of hydrogen storage materials. *Solar Compass*, *5*, 100033; https://doi.org/10.1016/j.solcom.2023.100033

Ostadi, M., Rytter, E., & Hillestad, M. (2019). Boosting carbon efficiency of the biomass to liquid process with hydrogen from power: The effect of H2/CO ratio to the Fischer-Tropsch reactors on the production and power consumption. *Biomass and Bioenergy*, *127*, 105282; https://doi.org/10.1016/j.biombioe.2019.105282

Pal, D. B., Chand, R., Upadhyay, S. N., & Mishra, P. K. (2018). Performance of water gas shift reaction catalysts: A review. *Renewable and Sustainable Energy Reviews*, *93*, 549-565; https://doi.org/10.1016/j.rser.2018.05.003

Pambudi, N. A., Firdaus, R. A., Rizkiana, R., Ulfa, D. K., Salsabila, M. S., Suharno, & Sukatiman. (2023). Renewable Energy in Indonesia: Current Status, Potential, and Future Development. *Sustainability*, *15*(3), 2342; https://www.mdpi.com/2071-1050/15/3/2342

Peng, W. X., Wang, L. S., Mirzaee, M., Ahmadi, H., Esfahani, M. J., & Fremaux, S. (2017). Hydrogen and syngas production by catalytic biomass gasification. *Energy Conversion and Management*, *135*, 270-273; https://doi.org/10.1016/j.enconman.2016.12.056

Plyasova, L. M., Yur'eva, T. M., Kriger, T. A., Makarova, O. V., Zaikovskii, V. I., Solov'eva, L. P., & Smhakov, A. N. (1995). Formation of a catalyst for methanol synthesis. *Kinetics and Catalysis*, *36*, 425-433;

Poggio-Fraccari, E., Abele, A., Zitta, N., Francesconi, J., & Mariño, F. (2022). CO removal for hydrogen purification via Water Gas Shift and COPROX reactions with monolithic catalysts. *Fuel*, *310*, 122419; https://doi.org/10.1016/j.fuel.2021.122419

Qin, R., Liu, P., Fu, G., & Zheng, N. (2018). Strategies for Stabilizing Atomically Dispersed Metal Catalysts. *Small Methods*, *2*(1), 1700286; https://doi.org/10.1002/smtd.201700286

Ratnawati, R., Slamet, S., Toya, F. D., & Kuntolaksono, S. (2022). Enhancing Hydrogen Generation using CdS-modified TiO2 Nanotube Arrays in 2,4,6-Trichlorophenol as a Hole Scavenger [2,4,6-Trichlorophenol; Hole Scavenger; Hydrogen Evolution; Titania Nanotube Arrays; TNTA-CdS]. *International Journal of Renewable Energy Development*, *11*(4), 9; https://doi.org/10.14710/ijred.2022.45139

Reddy, G. K., & Smirniotis, P. G. (2015) Water Gas Shift Reaction: Chapter 3 - Low-Temperature WGS Reaction, pp. 47-100. Elsevier. https://doi.org/10.1016/B978-0-12-420154-5.00003-6

Peraturan Pemerintah Republik Indonesia Nomor 79 Tahun 2014 Tentang Kebijakan Energi Nasional, (2014).

Saeidi, S., Fazlollahi, F., Najari, S., Iranshahi, D., Klemeš, J. J., & Baxter, L. L. (2017). Hydrogen production: Perspectives, separation with special emphasis on kinetics of WGS reaction: A state-of-the-art review. *Journal of Industrial and Engineering Chemistry*, *49*, 1-25; https://doi.org/10.1016/j.jiec.2016.12.003

Sahrin, N. T., Shiong Khoo, K., Wei Lim, J., Shamsuddin, R., Musa Ardo, F., Rawindran, H., Hassan, M., Kiatkittipong, W., Alaaeldin Abdelfattah, E., Da Oh, W., & Kui Cheng, C. (2022). Current perspectives, future challenges and key technologies of biohydrogen production for building a carbon–neutral future: A review. *Bioresource Technology*, *364*, 128088; https://doi.org/10.1016/j.biortech.2022.128088

Sansaniwal, S. K., Pal, K., Rosen, M. A., & Tyagi, S. K. (2017). Recent advances in the development of biomass gasification technology: A comprehensive review. *Renewable and Sustainable Energy Reviews*, *72*, 363-384; https://doi.org/10.1016/j.rser.2017.01.038

Sengupta, S., & Deo, G. (2015). Modifying alumina with CaO or MgO in supported Ni and Ni–Co catalysts and its effect on dry reforming of CH4. *Journal of CO2 Utilization*, *10*, 67-77; https://doi.org/10.1016/j.jcou.2015.04.003

Shen, X., Li, Z., Xu, J., Li, W., Tao, Y., Ran, J., Yang, Z., Sun, K., Yao, S., Wu, Z., Rac, V., Rakic, V., & Du, X. (2023). Upgrading the low temperature water gas shift reaction by integrating plasma with a CuOx/CeO2 catalyst. *Journal of Catalysis*, *421*, 324-331; https://doi.org/10.1016/j.jcat.2023.03.033

Shim, J.-O., Na, H.-S., Jha, A., Jang, W.-J., Jeong, D.-W., Nah, I. W., Jeon, B.-H., & Roh, H.-S. (2016). Effect of preparation method on the oxygen vacancy concentration of CeO2-promoted Cu/γ-Al2O3 catalysts for HTS reactions. *Chemical Engineering Journal*, *306*, 908-915; https://doi.org/10.1016/j.cej.2016.08.030

Shuai, C., Hu, S., He, L., Xiang, J., Su, S., Sun, L., Jiang, L., Wang, Y., Chen, Q., Liu, C., & Chi, H. (2015). Performance of CaO for phenol steam reforming and water–gas shift reaction impacted by carbonation process. *International Journal of Hydrogen Energy*, *40*(39), 13314-13322; https://doi.org/10.1016/j.ijhydene.2015.07.167

Smith. J.B.R., Loganathan, M., & Shantha, M. S. (2010). A Review of the Water Gas Shift Reaction Kinetics. *International Journal of Chemical Reactor Engineering*, *8*(1); https://doi.org/10.2202/1542-6580.2238

Song, J. H., Han, S. J., Yoo, J., Park, S., Kim, D. H., & Song, I. K. (2016). Hydrogen production by steam reforming of ethanol over Ni–X/Al2O3–ZrO2 (X=Mg, Ca, Sr, and Ba) xerogel catalysts: Effect of alkaline earth metal addition. *Journal of Molecular Catalysis A: Chemical*, *415*, 151-159; https://doi.org/10.1016/j.molcata.2016.02.010

Speight, J. G. (2019) Heavy Oil Recovery and Upgrading: Chapter 15 - Hydrogen Production, pp. 657-697. Gulf Professional Publishing. https://doi.org/10.1016/B978-0-12-813025-4.00015-5

Stiegel, G. J., & Ramezan, M. (2006). Hydrogen from coal gasification: An economical pathway to a sustainable energy future. *International Journal of Coal Geology*, *65*(3), 173-190; https://doi.org/10.1016/j.coal.2005.05.002

Taniya, K., Horie, Y., Fujita, R., Ichihashi, Y., & Nishiyama, S. (2023). Mechanistic study of water–gas shift reaction over copper/zinc-oxide/alumina catalyst in a reformed gas atmosphere: Influence of hydrogen on reaction rate. *Applied Catalysis B: Environmental*, *330*, 122568; https://doi.org/10.1016/j.apcatb.2023.122568

Tian, Z., Lu, Y., Wang, J., Shu, R., Wang, C., & Chen, Y. (2024). Advances in hydrogen production by aqueous phase reforming of biomass oxygenated derivatives. *Fuel*, *357*, 129691; https://doi.org/10.1016/j.fuel.2023.129691

Tleubergenova, A., Han, B.-C., & Meng, X.-Z. (2024). Assessment of biomass-based green hydrogen production potential in Kazakhstan. *International Journal of Hydrogen Energy*, *49*, 349-355; https://doi.org/10.1016/j.ijhydene.2023.08.197

Veziroğlu, T. N., & Şahi˙n, S. (2008). 21st Century's energy: Hydrogen energy system. *Energy Conversion and Management*, *49*(7), 1820-1831; https://doi.org/10.1016/j.enconman.2007.08.015

Wang, K., Khoo, K. S., Chew, K. W., Selvarajoo, A., Chen, W.-H., Chang, J.-S., & Show, P. L. (2021). Microalgae: The Future Supply House of Biohydrogen and Biogas [Mini Review]. *Frontiers in Energy Research*, *9*; https://doi.org/10.3389/fenrg.2021.660399

Watanabe, M. D. B., Cherubini, F., Tisserant, A., & Cavalett, O. (2022). Drop-in and hydrogen-based biofuels for maritime transport: Country-based assessment of climate change impacts in Europe up to 2050. *Energy Conversion and Management*, *273*, 116403; https://doi.org/10.1016/j.enconman.2022.116403

Watson, J., Zhang, Y., Si, B., Chen, W.-T., & de Souza, R. (2018). Gasification of biowaste: A critical review and outlooks. *Renewable and Sustainable Energy Reviews*, *83*, 1-17; https://doi.org/10.1016/j.rser.2017.10.003

Xiang, Y., He, J., Sun, N., Fan, Y., Yang, L., Fang, C., & Kuai, L. (2020). Hollow mesoporous CeO2 microspheres for efficient loading of Au single-atoms to catalyze the water-gas shift reaction. *Microporous and Mesoporous Materials*, *308*, 110507; https://doi.org/10.1016/j.micromeso.2020.110507

Yan, X., Li, Y., Zhang, C., Wang, Y., Zhao, J., & Wang, Z. (2021). Understanding the enhancement of CaO on water gas shift reaction for H2 production by density functional theory. *Fuel*, *303*, 121257; https://doi.org/10.1016/j.fuel.2021.121257

Yana, S., Nizar, M., Irhamni, & Mulyati, D. (2022). Biomass waste as a renewable energy in developing bio-based economies in Indonesia: A review. *Renewable and Sustainable Energy Reviews*, *160*, 112268; https://doi.org/10.1016/j.rser.2022.112268

Yao, S., Zhang, X., Zhou, W., Gao, R., Xu, W., Ye, Y., Lin, L., Wen, X., Liu, P., Chen, B., Crumlin, E., Guo, J., Zuo, Z., Li, W., Xie, J., Lu, L., Kiely, C. J., Gu, L., Shi, C., . . . Ma, D. (2017). Atomic-layered Au clusters on α-MoC as catalysts for the low-temperature water-gas shift reaction. *Science*, *357*(6349), 389-393; https://doi.org/10.1126/science.aah4321

Ye, J., Song, S., Cui, Z., Wu, P., Zhang, Y., Luo, W., Ding, T., Tian, Y., & Li, X. (2023). Facile Synthesis of Efficient and Robust Cu–Zn–Al Catalysts by the Sol–Gel Method for the Water–Gas Shift Reaction. *Industrial & Engineering Chemistry Research*, *62*(38), 15386-15394; https://doi.org/10.1021/acs.iecr.3c01333

Younas, M., Shafique, S., Hafeez, A., Javed, F., & Rehman, F. (2022). An Overview of Hydrogen Production: Current Status, Potential, and Challenges. *Fuel*, *316*, 123317; https://doi.org/10.1016/j.fuel.2022.123317

Zhang, F., Liu, Y., Xu, X., Yang, P., Miao, P., Zhang, Y., & Sun, Q. (2018). Effect of Al-containing precursors on Cu/ZnO/Al2O3 catalyst for methanol production. *Fuel Processing Technology*, *178*, 148-155; https://doi.org/10.1016/j.fuproc.2018.04.021

Zhou, L., Liu, Y., Liu, S., Zhang, H., Wu, X., Shen, R., Liu, T., Gao, J., Sun, K., Li, B., & Jiang, J. (2023). For more and purer hydrogen-the progress and challenges in water gas shift reaction. *Journal of Energy Chemistry*, *83*, 363-396; https://doi.org/10.1016/j.jechem.2023.03.055

Zhu, M., Tian, P., Kurtz, R., Lunkenbein, T., Xu, J., Schlögl, R., Wachs, I. E., & Han, Y.-F. (2019). Strong Metal–Support Interactions between Copper and Iron Oxide during the High-Temperature Water-Gas Shift Reaction. *Angewandte Chemie International Edition*, *58*(27), 9083-9087; https://doi.org/10.1002/anie.201903298

Zhu, M., & Wachs, I. E. (2016). Iron-Based Catalysts for the High-Temperature Water–Gas Shift (HT-WGS) Reaction: A Review. *ACS Catalysis*, *6*(2), 722-732; https://doi.org/10.1021/acscatal.5b02594

Živković, L. A., Pohar, A., Likozar, B., & Nikačević, N. M. (2016). Kinetics and reactor modeling for CaO sorption-enhanced high-temperature water–gas shift (SE–WGS) reaction for hydrogen production. *Applied Energy*, *178*, 844-855; https://doi.org/10.1016/j.apenergy.2016.06.071